MADRID
inter.noise 2019
June 16 - 19
NOISE CONTROL FOR A BETTER ENVIRONMENT

Active structural excitation as known source for structure-borne noise research

Norambuena, Marco[1] and Winter, René[2]
[1,2] German Aerospace Center (DLR), Institute of Aeroelasticity
Bunsenstr. 10, D-37073, Göttingen, Germany

ABSTRACT

An important element required to investigate structure-borne noise propagation mechanisms is the ability to have full knowledge and control over the excitation sources responsible for the disturbance. Such information can help to understand propagation and radiation of energy once known forces are introduced into the structure. However precise control over structural excitation tends to be disregarded and generalized to simple broadband excitation. Cabin noise research could benefit from having the ability to reproduce on the structure a more realistic excitation, such as engine induced vibrations. Moreover, being able to reproduce engine excitation under laboratory conditions can be highly beneficial and could potentially allow to perform, from the vibro-acoustic point of view, flight tests on the ground. If the idea is to inject into the structure an exact copy of an arbitrary reference force signal, an active controller can be used in order to compensate force signals to obtain such copy at the injection point on the structure. The system developed is able to perform simultaneously the system identification and the control of injected forces. The following work describes the adaptive MIMO controller implemented for such an objective and discusses test results obtained in the laboratory.

Keywords: Active, Vibration, Excitation
I-INCE Classification of Subject Number: 48

1. INTRODUCTION

In the aeronautics industry, Ground Vibration Tests (GVT's) are a well stablished testing procedure meant to characterize structural behavior of aircrafts. Such applied methodology serves as key part not only in the understanding of aeroelastic stability but also provides relevant data used to validate analytical models that ultimately become part of the certification process of airworthiness [1]. In summary, GVT's are able to accurately describe the fuselage response by means of artificial excitation of the structure. There are two other closely related methods to achieve similar objectives, Taxi Vibrations Tests (TVT) and Flight Vibrations Tests (FVT), the former consists in the replacement of the artificial shaker excitation by the natural vibrations generated during aircraft taxiing [2] and the later uses the operational vibration generated on the fuselage during flight [3].

Any current structural testing procedure in the field of aeronautics uses one, or a variation, of these methods. From the excitation point of view, the most common

[1]Marco.Norambuena@dlr.de
[2]Rene.Winter@dlr.de

strategy is to use arbitrary, but known, excitation signals, e.g. white noise or sine sweeps. This provides the necessary flexibility to obtain, for instance, frequency response functions, modal parameters, etc.

One could easily argue that a FVT will provide the perfect type of excitation since it is in fact an operational condition, however the elevated costs associated with flight tests make this option unfeasible in most cases. Moreover, such type of excitation, although ideal for many applications, is completely unknown and difficult to quantify since there are multiple sources acting on the fuselage during flight. The unavailability of such excitation reference will limit the types of processing that can be performed, e.g. modal masses can't be obtained.

During recent years [4], vibroacoustic topics had drawn considerable attention in the aeronautic industry. This is given by the fact that concerns have been shifted from safety and reliability topics of previous decades of research to cabin quality and passenger comfort. This current trend has pushed the development of new tools and methodologies in order to face these new challenges [5]. A set of refocused topics has emerged from the interest in understanding how vibroacoustics play a crucial role in the cabin noise.

Given the fact that the starting points of all vibroacoustic phenomena are vibrations propagating on a structure, it is necessary to have a suitable excitation system capable of reproduce real flight operational conditions. If we forget for one second the effect of the Turbulent Boundary Layer, the solely source responsible for vibrations on the fuselage at low frequencies are the loads generated by the rotating components of the engines.

Through simulation, it is possible to accurately calculate the loads generated at connection points between engines and fuselage. However, a key problem arises at the moment when you try to reproduce those loads on the structure, since there is no way to compensate for the modifications introduced by the system created between amplifier, shaker and structure. Such unaccounted system will certainly change the predefined reference loads. Nonetheless, if the reference loads signal is available, it can be used to design an active excitation system able to generate and inject into the structure an exact copy of the simulated loads. As we will show in the following sections, such real-time excitation system is based on an adaptive controller. As part of the development process, as a first step a single-input single-output (SISO) controller was investigated and implemented. The fundamentals of this system served later on as a stepping stone for the more complex multi-input multi-output (MIMO) controller. Such multichannel system is part of our long-term goal to create a system able to reproduce forces in the three directions of space plus its associated moments.

Therefore, if we could implement a system able to excite a structure in a realistic manner, mimicking true loads, such system will allow to study the vibroacoustic behavior of a structure in the most accurate way possible. Such opportunity will help, for example, in the better understanding of structure—borne noise mechanisms of different parts of a fuselage or will assist in the determination of relevant energy transmission paths between sources and receivers.

2. CONTROLLED EXCITATION

The type of problem presented in this scenario, where it is required to inject on a structure a copy of an arbitrary reference force signal, seems to be a perfect candidate for an active control solution. The two main reasons for this are the availability of a reference signal, in this case the load forces, and the need to compensate a relatively stable plant. In this particular case the plant consists of the path created between

amplifier, electrodynamic shaker, the structure and a force cell used to quantify the injected force, Figure 1 shows the configuration of the plant.

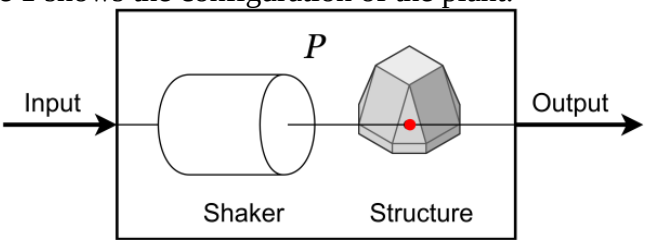

Figure 1: Schematic of the plant which consists of a shaker, a structure and a force cell (denoted by the red dot) that quantify the injected force into the structure.

The type of configuration described above is known as inverse control, since the task of adaptive process is to generate an inverse system $\hat{C}$ of the plant *P*. If this is successfully accomplished, the output of the plant will be an unmodified copy of the reference force signal. The typical schematic of an idealized inverse controller is shown in Figure 2, where $\hat{C}$ represents the compensation filter of the plant *P*, driven by the adaptive procedure. The error signal represents the deviation of the output of the plant in comparison with the reference force signal at the input of $\hat{C}$.

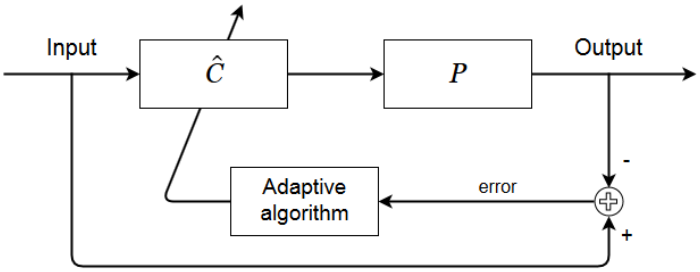

Figure 2: Block diagram of an idealized adaptive inverse controller.

There are multiple options available to implement the adaptive algorithm. From the most simple and reliable LMS variations to the most sophisticated and demanding RLS variations.

According with this type of application, the following algorithms were tested in order to find the best tradeoff between speed of convergence and overall quality of output signal: NLMS, Correlation-LMS, DCT-LMS and RLS. The comparisons showed that all algorithms performed fairly well. After this comparison and considering that there is no requirement of high speed tracking of the reference signal, it was decided that the NLMS was the proper choice at this stage. Having the simplicity of an NLMS algorithm will make it easier to debug any problem that could potentially appear during the implementation on hardware.

The idealized system shown in Figure 2 is the most basic configuration for an inverse controller. However this simplicity helps to illustrate how such configuration works. Unfortunately, such idealized controller is not able to work properly on a real implementation since it requires conditions that are almost impossible to obtain, e.g. that there is no internal disturbance at the output of *P*. One of the options suggested in the literature [6] that can be used for an actual implementation, has a configuration similar to what is called *filtered-x* LMS (Fx-LMS) algorithm. This configuration is well known and widely used in Active Noise Control applications [7].

One of the characteristics of this configuration is that the control filter $\hat{C}$ is not applied directly to the plant P but rather to a modeled version $\hat{P}$ of the plant. The Fx-NLMS configuration ensures stable inverse control of the plant even in the case where there are errors in the modeling of $\hat{P}$. Independently of how $\hat{P}$ is modeled, online or offline, the complete control system can be summarized in Figure 3. In this schema it is assumed that on a previous process the plant $\hat{P}$ was identified and now a copy is connected at the input of the control filter $\hat{C}$. Under certain conditions it could be desired that the plant does not track directly the *Reference* signal but rather a delayed or modified version of the *Reference*. The introduction of the *Reference model M* serves this purpose.

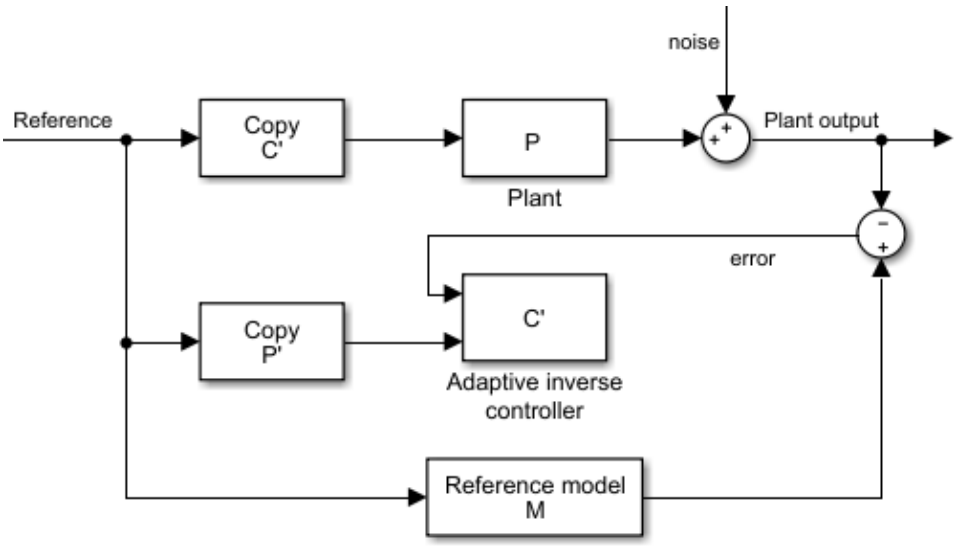

Figure 3: Block diagram of inverse controller with added reference model.

3. SIMULATIONS

Although multiple simulations were performed during the development processes in order to test different algorithms, a simple example is presented here for the purpose of illustrating the general behavior of the controller. In this example, an arbitrary plant *P* with a low-pass characteristic was chosen. This fact is evidenced by the spectral profile of the *Control OFF* curve in Figure 5, which will be discussed shortly. The reference signal was defined as the sum of four sinusoids with frequencies 30, 50, 170 and 240 Hz.

In the following figures, time and frequency comparisons are presented between the *Reference* that represents the desired signal that should be injected into the structure, *Control OFF* that represents the signal obtained at the output of the plant when no control is performed (bypassing $\hat{C}$) and *Control ON* is the same as the latter but now the controller $\hat{C}$ is operating. All these curves are shown in Figure 4 and Figure 5. The time domain comparison, in Figure 4, presents two important characteristics, firstly, the evident difference between the *Reference* signal and the *Control OFF* signal given by the effect of the transfer function of the plant *P*. This means that when there is no control applied, the injected signal into the structure does not resemble the predefined *Reference* signal. The second characteristic worth to mention is the evolution of the *Control ON* signal and its convergence to the *Reference* signal as time passes. This means that, as it was designed, after some time the controller $\hat{C}$ will compensate the influence of the plant *P* and will inject a proper copy of the *Reference* signal into the structure. The spectral comparison presented in Figure 5 shows a similar result, a

disparity between *Reference* and *Control OFF* signals; and subsequently a perfect matching between *Reference* and *Control ON* signals.

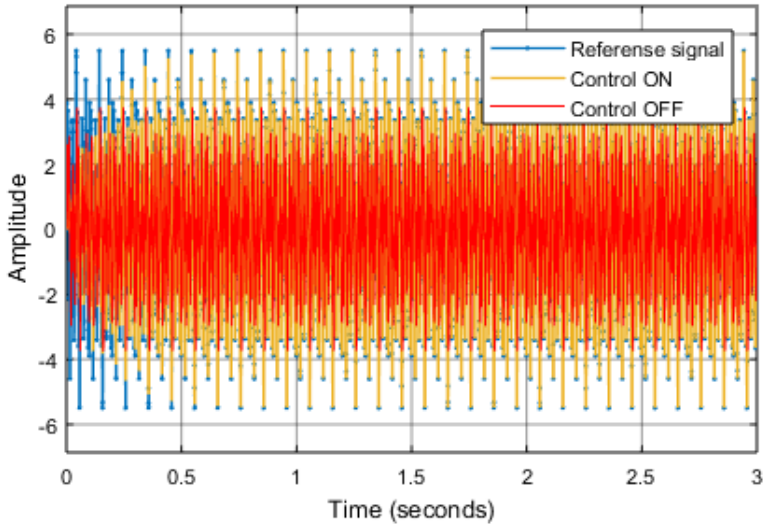

Figure 4: Comparison of signals evolution.

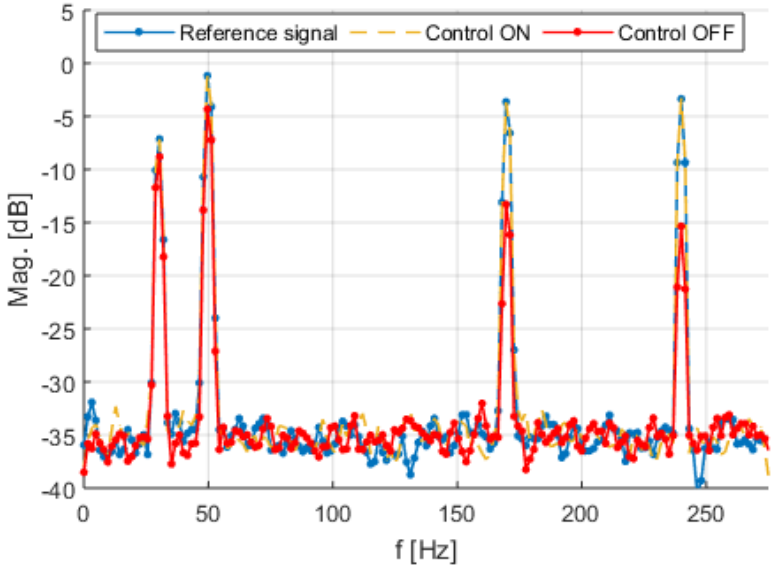

Figure 5: Comparison of resulting spectra.

The task performed by the adaptive filter $\hat{C}$ can be described by the evolution of its coefficients. Equally important, at the core of the adaptive process is the evolution of the error signal, which is responsible for driving the coefficients of $\hat{C}$ in the update equation of the LMS algorithm. The relationship between the progression of the error and the controller $\hat{C}$ can be observed in Figure 6.

4. HARDWARE REALIZATION AND EXPERIMENTAL RESULTS OF A SISO SYSTEM

The last stage in the development process of the active controller was the implementation of the previously described algorithm into specialized hardware running in real time. The whole controller was implemented in two separate steps, firstly the plant P was identified and then a copy of P was used to run the Fx-NLMS inverse

control. For this purpose the algorithm was developed using Simulink and an ADwin-Pro II T12 system.

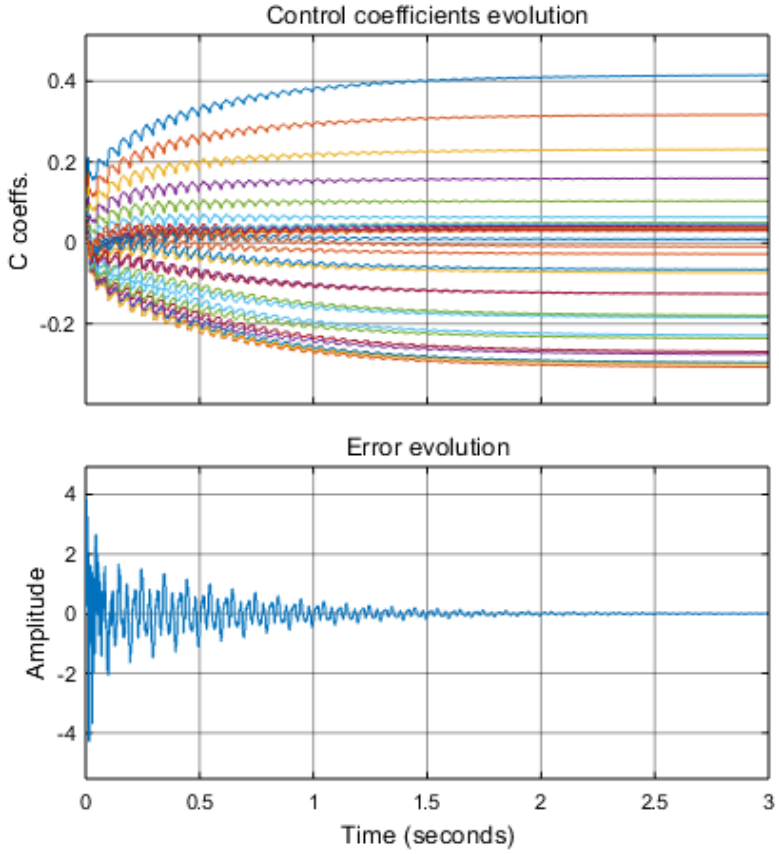

Figure 6: Illustration of error and coefficients evolution of the presented simulation.

In order to evaluate the correct operation of the system, a laboratory experiment was designed. The idea was to define a reference signal with a narrow band profile that resembles a low pass filter characteristic but with a non-flat response, as seen in Figure 7. In this way, the performance of the controller will be evaluated under, although limited, broadband condition that is still relevant for the use cases of structural excitation. The chosen frequency range was from 0 to 120 Hz.

The test structure used was a single aluminum plate of 1 x 0.8 x 0.03 m, with an asymmetric milled pattern that resembles the skin fields, stringers and frames typically found in fuselage structures. The thickness of the skin fields, stringers and frames was 1, 5 and 10 mm respectively. The plate was suspended using bungee cords in order to generate free displacement boundary conditions. As seen in Figure 8, a shaker and an impedance head were screwed to an anchor point of the plate. From the impedance head, the force signal was used to generate the error signal by comparing the actual injected force with the predefined force reference signal.

A spectral comparison of the reference and control signals is shown in Figure 7; there it is possible to assess the correct operation of the controller under narrow band excitation. In addition, a second evaluation is made by calculating the transfer function between the input and the output of the whole system, from the *Reference* signal fed into the controller $\hat{C}$ up to the output of the plant using the signal coming from the force cell. As before, two conditions are evaluated, *Control ON* and *OFF*. The comparison of the frequency response function for both conditions is made in terms of their magnitude and phase, as shown in Figure 9. The results presented there provide evidence about the

correct operation of the controller. Firstly, the adjustment of the magnitude around 1 means a close match between the injected force into the structure and the predefined reference. Secondly, a similar behavior takes place with the phases of both cases, where the *Control ON* condition displays a relatively flat line around 0 rad. All this means that the controller is properly working and is able, for the most part, to calibrate the injected force using the predefined *Reference* signal.

There are, however, three distinctive peaks that appear in the higher frequency region, this peaks are associated with the natural modes of the plate. Their presence there is somewhat expected; it is possible to identify two important factors that can influence their appearance here. In the first place, the structure used is highly undamped which can greatly increase the interaction between the injected force and response of the plate. Near resonances, any small out-of-phase displacement between the structure and the force cell can generate a seemingly large signal at the output of the force cell. Secondly, the assumption that the shaker is behaving as a linear time invariant (LTI) system is not necessarily true, at least up to some degree. One option to minimize this effect could be to perform an online identification of the plant $\hat{P}$ in order to compensate any variation over time while the inverse controller is running.

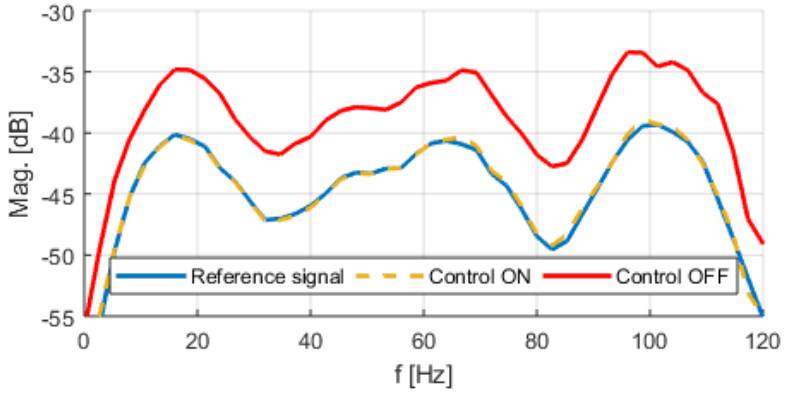

Figure 7: Spectral comparison of reference and control signals.

Figure 8: Aluminum plate used as test structure in a SISO configuration.

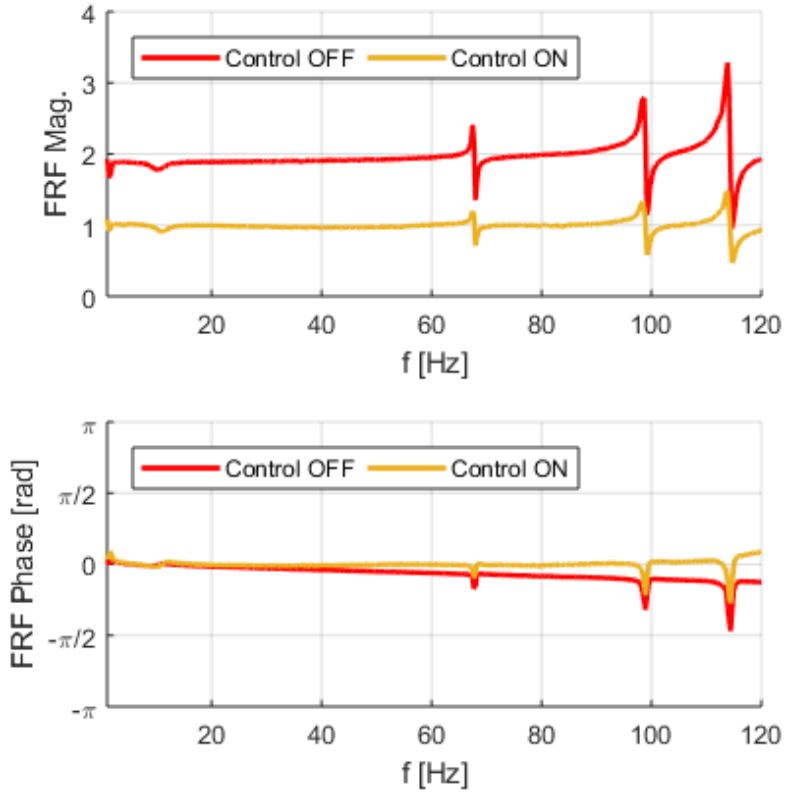

Figure 9: Frequency response function comparison in terms of magnitude and phase relatively to the reference signal.

5. HARDWARE REALIZATION AND EXPERIMENTAL RESULTS OF A MIMO SYSTEM

The next step in the development of the system was to extend its capabilities to be able to provide three-dimensional controlled excitation, i.e. in each direction of space. The extension from a SISO controller, as described previously, to a MIMO implementation required certain modifications of the algorithms. The previously shown implementation relies on the fact that SISO system are commutative, i.e. $P(z)\,C(z) = C(z)\,P(z)$. However, such a property is in general not true for MIMO systems as pointed out by Plett [8]. Special care needs to be taken in the order of how the transfer function matrix of the controller C is manipulated. Plett also introduces a highly efficient controller by using a Recursive Least Square (RLS) update strategy. It is a well-known fact that RLS algorithms, although fast, are computationally demanding. During the development phase it was clear that the AD-win system was not able to run the controller at the required sampling rate with a RLS algorithm. Therefore, a simplified version was implemented with an LMS algorithm, in a similar manner as the SISO controller. The cost of this decision is carried by the speed of convergence, however for our application it has a low impact if we have to wait a little longer before the control coefficients settle and the optimal solution is reached.

Two incremental versions of the MIMO controller were developed during this part of the project. The first version took a simple approach similar to the SISO system in the sense that there were two steps for the controller to work. In the initial step the mimo plant P was identified and the corresponding coefficient stored. The second step consisted in loading the stored coefficients of P to use them as part of the inverse controller. This approach ensured a simple structure that could help to debug any potential problem during development. Later on, a second version was implemented

with a more advanced approach. In this case, both previous steps were merged into a single algorithm that performed simultaneously the system identification of *P* while the inverse control was operating. The scheme used is shown in Figure 10, where the blocks naming are similar to the SISO system introduced in Figure 3. Further specifics of this control strategy can be found in Plett's reference. Since this is a controller driven by a reference system, and not a reference signal, the inputs r_k and n_k correspond to broadband noise. In principle both developed version used the same reference model *M*, still due to changes in the sampling frequency and how these models are created, small differences occurred. This means that, although both reference models do not match perfectly, they follow a resembling frequency profile as will be seen in Figure 12 and Figure 13. Nonetheless, for our comparison these small differences are irrelevant and only a global qualitative performance is derived from both versions.

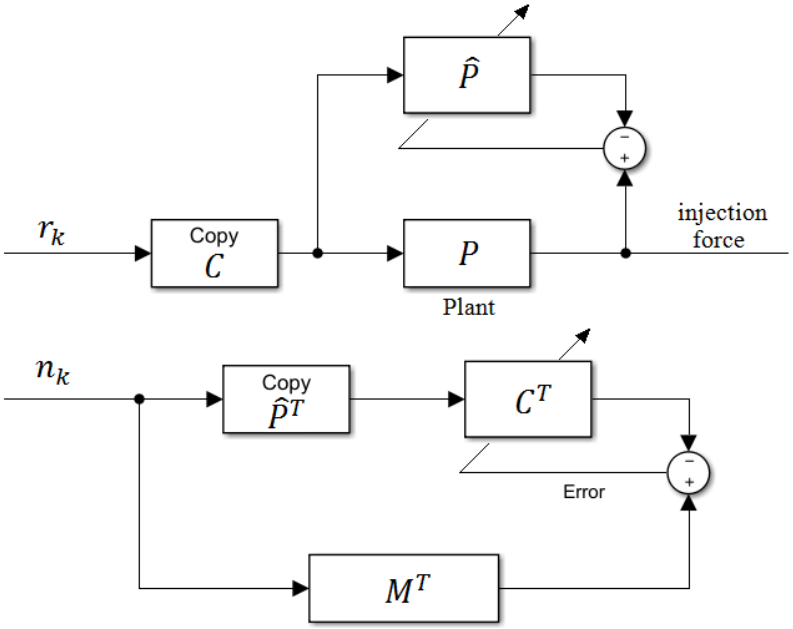

Figure 10: Block diagram of MIMO hybrid controller.

For the evaluation of the MIMO implementation, the same aluminum plate was used but this time three shakers were attached, one per spatial direction as seen in Figure 11. In this case, three different frequency profiles were arbitrarily defined. As in the previous SISO case, these profiles serve as the target reference that the controller will try to replicate at the injection point of the structure. The profiles were integrated into the controller as part of the reference model *M*. The results of the evaluation are summarized in Figure 12 and Figure 13, where the *Reference* profiles and the *Control ON* condition are shown. There, each color represents one direction in space, the solid and dashed lines represent the *Reference* and the *Control ON* respectively. From Figure 12 it is possible establish the correct operation of the controller. The good agreement among references and resulting profiles illustrates the proper generation of control coefficients and the successful application of the compensation filter *C* to the input signal. In X direction, it is possible to notice a relatively small difference of 0.6 dB between *Reference* and *Control ON* in the region of interest. In Y direction, vertical excitation, the difference between both curves seems to increase in the upper frequency range. We assume that in this direction the suspension of the plate negatively affects the result. It is not unreasonable to assume that a non-linear effect of the bungee cords suspension escapes the control capabilities of the system making it appear as a less

favorable result. In order to validate this assumption, a new configuration of suspension is being designed to minimize its influence and will be evaluated in the near future. The Z direction, perpendicular to the plate, presents an almost perfect match between *Reference* and *Control ON* profiles. The results of the second version of the controller, shown in Figure 13, exceed its predecessor. In this case there is a closer match between *References* and *Control ON* condition in all three directions. Despite this better agreement, once again it is possible to observe a small deviation region in the Y curve. As already discussed, this may be caused by the suspension system of the plate. Nevertheless, the important outcome if this comparison is that the second version of the controller performs substantially better, this is most probably due to the continuous adjustment of the identified plant that quantifies any deviation occurring during the operation of the controller.

Figure 11: Aluminum plate with MIMO configuration.

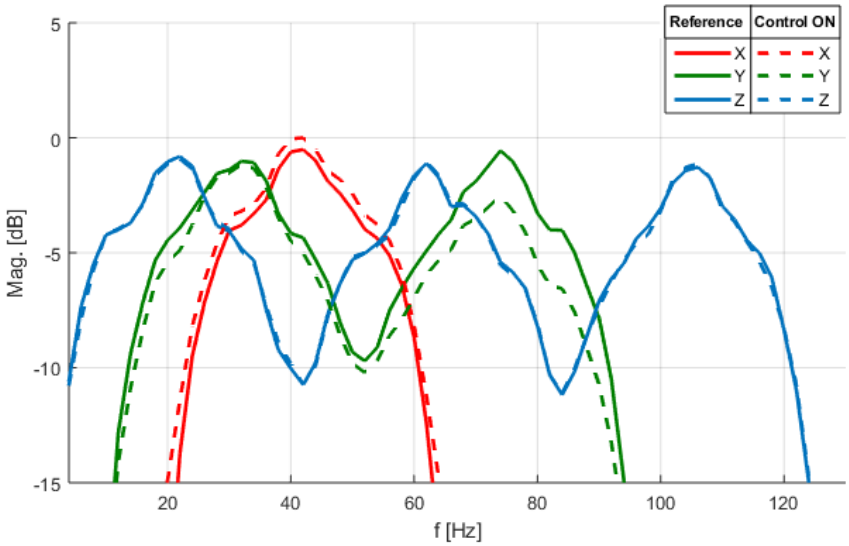

Figure 12: Spectral comparison of first version of MIMO controller, references vs. control ON condition.

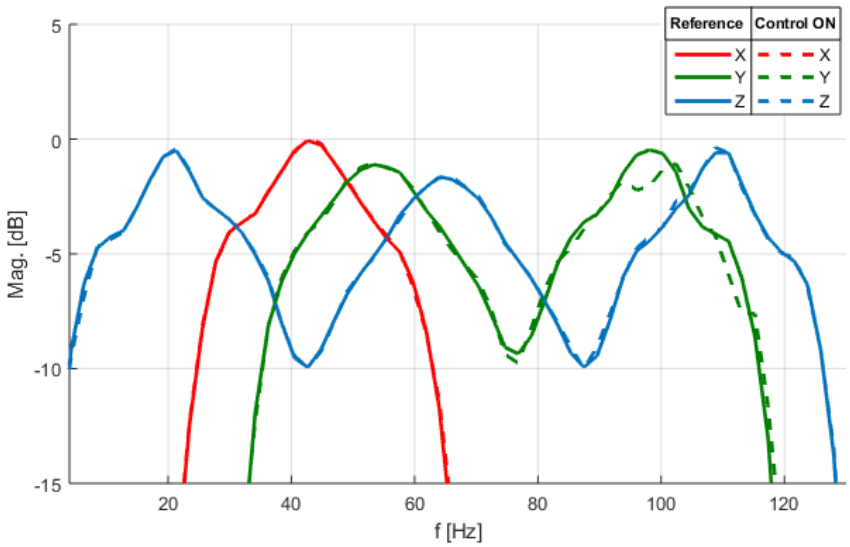

Figure 13: Spectral comparison of second version of MIMO controller, references vs. control ON condition.

6. CONCLUSIONS

In this paper we examine the application of an active system to perform controlled structural excitation. Simulations and laboratory test show that it is possible to successfully apply a calibrated excitation for either multi-tonal or broadband signals in accordance with an arbitrary predefined signal reference or model reference. A SISO and a more sophisticated MIMO controller were presented and evaluated. The successful implementation of both configurations was demonstrated through laboratory experiments. Both controllers were able to reproduce reference forces with great accuracy. Moreover, two versions of MIMO controllers were implemented as part of the development within this project. The most advanced version of the MIMO controller showed significant better performance than its predecessor.

Future work will move forward by extending the current system to be able to control moments.

7. ACKNOWLEDGEMENT

This project has received funding from the Clean Sky 2 Joint Undertaking under the European Union's Horizon 2020 research and innovation programme under grant agreement N° CS2-LPA-GAM-2014-2015-01.

8. REFERENCES

[1] D. Göge, M. Böswald, U. Fullekrug and L. Pascal, "Ground Vibration Testing of Large Aircraft - State-of-the-Art and Future Perspectives," in *Proceedings of the 25th International Modal Analysis Conference (IMAC XXV)*, Orlando, 2007.

[2] M. Böswald and Y. Govers, "Taxi Vibration Testing - An Alternative Method to Ground Vibration Testing of Large Aircraft," in *Proceedings of the International Conference on Noise and Vibration Engineering - ISMA 2008*, Leuven, 2008.

[3] J. Meijer, "Introduction to Flight Test Engineering - "Aeroelasticity"," RTO AGARDograph 300 Vol. 14, 2005.

[4] J. Biedermann, R. Winter, M. Norambuena and M. Böswald, "Classification of the mid-frequency range based on spatial Fourier decomposition of operational deflection shapes," in *24th International Congress on Sound and Vibration (ICSV24)*, London, 2017.

[5] R. Winter, J. Biedermann, M. Böswald and M. Wandel, "Dynamic characterization of the A400M acoustics fuselage demonstrator," in *Inter-Noise 2016*, Hamburg, 2016.

[6] B. Widrow and E. Walach, Adaptive Inverse Control, Prentice-Hall Inc., 1995.

[7] S. Elliott, Signal Processing for Active Control, London: Academic Press, 2001.

[8] G. Plett, "Efficient linear MIMO adaptive inverse control," *Adaptation and learning in control and signal processing*, vol. 34, no. 14, pp. 89-94, 2001.